Cement and Concrete Research 41 (2011) 1357–1367

Contents lists available at ScienceDirect

Cement and Concrete Research

journal homepage: http://ees.elsevier.com/CEMCON/default.asp

Modeling of early age behavior of blast furnace slag concrete based on micro-physical properties

Tetsuya Ishida [a,*], Yao Luan [a], Takahiro Sagawa [b], Toyoharu Nawa [c]

[a] Department of Civil Engineering, The University of Tokyo, 7-3-1, Hongo, Bunkyo-ku, Tokyo, 113-8656, Japan
[b] Technical Development Lab., Nittetsu Cement Co., Ltd., 64, Nakamachi, Muroran, 050-8510, Japan
[c] Division of Sustainable Resources Engineering, Graduate School of Engineering, Hokkaido University, North13-West8, Kita-ku, Sapporo, 060-8628, Japan

ARTICLE INFO

Article history:
Received 2 November 2010
Accepted 7 June 2011

Keywords:
Blast furnace slag [D]
Porosity
Pore size distribution [B]
Strength [C]
Drying shrinkage [A]

ABSTRACT

A multi-scale system called DuCOM was enhanced to model behaviors of blast furnace slag (BFS) concrete. Tests on the strength and micro–hygro–physical properties of BFS concrete and Portland cement concrete were conducted. The current model was found to underestimate the strength of BFS concrete at later ages owing to underestimation of the water content inside C–S–H gel pores. To remedy this, enhanced modeling of porosity allowing proper simulation of the porosity of the BFS paste matrix and higher strength development at later ages is proposed. Furthermore, based on the enhanced porosity model, the moisture loss and pore size distribution of the BFS paste matrix were investigated. The pore size distribution was found to be coarser than the test at later ages in the model, resulting in overestimation of moisture loss. Hence, the pore size distribution was enhanced as well, allowing simulation of a finer pore structure of the BFS matrix. Finally, verifications showed that the enhanced model better predicts water desorption, moisture loss and drying shrinkage behaviors.

1. Introduction

Blast furnace slag (BFS), which is a by-product obtained during steel manufacture, is widely used as a mineral admixture in cement in Japan. It is broadly recognized that BFS concrete has many advantages, including lower permeability, better chloride resistance and higher strength at later ages. However, some disadvantages are also reported [1–3], such as larger shrinkage that tends to induce cracking and decrease durability. Besides, when insufficient water is supplied during curing, the hydration process may be greatly retarded and the strength reduced significantly. Therefore, in order to promote broader application of blast furnace slag, further study of the properties of BFS concrete is in order.

Strength is regarded as one of the most valuable indexes in concrete engineering because it is associated with most other properties and can provide an overall indication of quality. Strength is closely tied to the reactivity of cement, and higher strength usually derives from a higher degree of hydration. However, when we switch to BFS blended cement from Portland cement concrete, it seems insufficient to attribute strength development only to the hydration process. For instance, it is well known that under room temperature when Portland cement (PC) is replaced partially by BFS, strength decreases at an early age while higher strength can be achieved at a later age. On the other hand, researchers [4–8] indicate that the hydration degree of slag ranges from 30% to 70% after long time curing such as 1–2 years, which is lower than that of Portland cement. Obviously BFS gains higher strength than PC at a later age, even if the hydration degree is lower than that of PC. This variance of strength could be explained by the pore structure of hardened cement paste. Microscopic observation [9–11] by Scanning Electron Microscopy (SEM) indicates that the BFS matrix with full curing has a denser structure than PC, and porosity analysis such as Mercury Intrusion Porosimetry (MIP) [12–15] also shows that at a later age the pore distribution curve moves towards a much finer diameter. Therefore, dense pore-structure can be considered to contribute more than hydration for the strength of BFS at later ages. Actually, other properties of BFS that differ from PC may be also related to the pore-structure. The moisture loss of BFS under drying conditions is reported to be less than that of PC [15,16], which can be explained by finer pores and stronger retention of water. It is also reported that drying shrinkage of BFS is larger than PC, especially for those cases with sufficient curing [17–20]. This larger shrinkage deformation can be attributed to the finer pore structure, because higher capillary tension force may be induced in the paste. Therefore, if one aims to evaluate or predict the macro-properties of BFS concrete based on micro-information, proper modeling and simulation of its microstructure are necessary.

At the Concrete Lab of the University of Tokyo, a computational system called DuCOM, which couples thermo–hygro–physical information of cementitious composites with a multi-scale constitutive model, has been developed by Maekawa et al. [21]. With this analytical system, properties over the whole life of concrete such as strength, shrinkage, creep, carbonation, and chloride penetration, can be predicted based on

* Corresponding author. Tel.: +81 3 5841 6102; fax: +81 3 5841 6010.
E-mail address: tetsuya.ishida@civil.t.u-tokyo.ac.jp (T. Ishida).

0008-8846/$ – see front matter © 2011 Elsevier Ltd. All rights reserved.
doi:10.1016/j.cemconres.2011.06.005

simulation of the degree of hydration, micro-pore structure, and moisture transport and equilibrium. This system has been verified for Portland cement concrete. As to BFS, some studies have also been conducted. For example, the authors have proposed the enhanced multi-component hydration model [22] for properly simulating the hydration process of slag in blended cement. However, with regard to the microstructure of BFS, the DuCOM system follows similar treatment with PC concrete, and the simulation has not been investigated and verified comprehensively by experiment results. Therefore, whether the DuCOM system is applicable to BFS concrete or needs any enhancement is still unknown.

The object of this research is to study and improve the current microstructure model in DuCOM, focusing on BFS concrete. It is expected that with the improvement of the current model for BSF concrete, the pore structure of the BFS matrix can be properly simulated. Furthermore, based on the correct information on pore-structure, prediction of the macro properties of BFS concrete such as strength and moisture loss could also be improved. Before that, the current microstructure model in DuCOM is introduced briefly in the following section.

2. Microstructure model and strength development

2.1. Microstructure model

In the microstructure model, micro-pore information mainly consists of two parts, i.e. porosity and pore size distribution. Fig. 1 shows the overall scheme of the model. According to their size, micro-pores in hardened paste are categorized into three types: capillary pores, gel pores, and interlayer pores. During the hydration process, hydration products, mainly C–S–H gel grains, are generated both inside and outside the cement particles. C–S–H grains precipitate outside cement particles and fill in large voids, and remains of these voids are categorized as capillary pores. Individual gel grains are considered to contain much smaller voids than capillary pores, called gel pores. Also, gel grains consist of numerous layers, and between those layers are extremely tiny spaces called interlayer pores, each of which is assumed to be accessible only by a single water molecule.

The interlayer (ϕ_{lr}), gel (ϕ_{gl}) and capillary (ϕ_{cp}) porosity are computed as follows:

$$\begin{aligned} V_s &= \frac{\alpha W_p}{1-\phi_{ch}}\left(\frac{1}{\rho_p}+\frac{\beta}{\rho_w}\right) \\ \phi_{lr} &= \left(t_w s_l \rho_g V_s\right)/2 \\ \phi_{gl} &= V_s\phi_{ch}-\phi_{lr} \\ \phi_{cp} &= 1-V_s-(1-\alpha)\left(W_p/\rho_p\right) \end{aligned} \tag{1}$$

where α is the hydration degree of cementitious powder, W_p is the weight of powder per unit paste volume, β is chemically combined water, ρ_p and ρ_w are the density of powder and chemically combined water, t_w is the interlayer pore diameter, which is the constant 2.8 Å, s_l is the specific surface area of the interlayer, ρ_g is the dry density of gel product, and ϕ_{ch} is the intrinsic porosity, which is the ratio of gel and interlayer porosity ($\phi_{lr}+\phi_{gl}$) to the volume of gel grain. ϕ_{ch} is considered as the intrinsic property of C–S–H and currently assumed to be the value of 0.33 under isothermal condition.

In order to evaluate pore size distribution, the pore surface area is required. For the surface area of capillary pores (S_c) and gel pores (S_g) per unit volume of matrix, the following equations are given:

$$\begin{aligned} S_c &= \int_{r_0}^{r_0+\delta_m} dS_c = \int \frac{4\pi r^2}{\zeta}\left(\frac{1-\phi_r}{1-\phi_{in}}\right)dr \\ S_g &= W_g s_g \end{aligned} \tag{2}$$

where δ_m is the cluster thickness of outer product at the instant of hydration, ϕ_{in} is the inner product porosity, r_0 is the average radius of cement particles, ϕ_r is the porosity at radius r, which is a function of r, ζ is the equivalent size of gel grains, and s_g is the internal specific surface area of gel particles. ζ and s_g are also regarded as intrinsic properties of C-S-H. Currently, s_g and ζ are assumed to be constant for Portland cement, and their values are 3.0×10^4 m^2/kg and 3.0×10^{-8} m.

The size distributions of capillary and gel pores are described by the following functions:

$$\begin{aligned} \phi_{cp}(r) &= \phi_{cp}\left(1-\exp\left(-B_{cp}r\right)\right) \\ \phi_{gl}(r) &= \phi_{gl}\left(1-\exp\left(-B_{gl}r\right)\right) \end{aligned} \tag{3}$$

where B_{cp} and B_{gl} are porosity distribution parameters for capillary and gel pores, respectively, which give the bridge connecting porosity and surface area by the following equation:

$$S_i = 2\phi_i \int_{r_{imn}}^{\infty} B_i \exp\left(-B_i r\right) d\ln r \tag{4}$$

where the subscript i represents *cp* or *gl*, i.e. capillary or gel. Based on the calculated porosity and surface area in Eqs. (1) and (2), B_{cp} and B_{gl} can be computed by Eq. (4).

Thus, the size distribution functions of capillary and gel pores in Eq. (3) are computed separately, and their superposition with

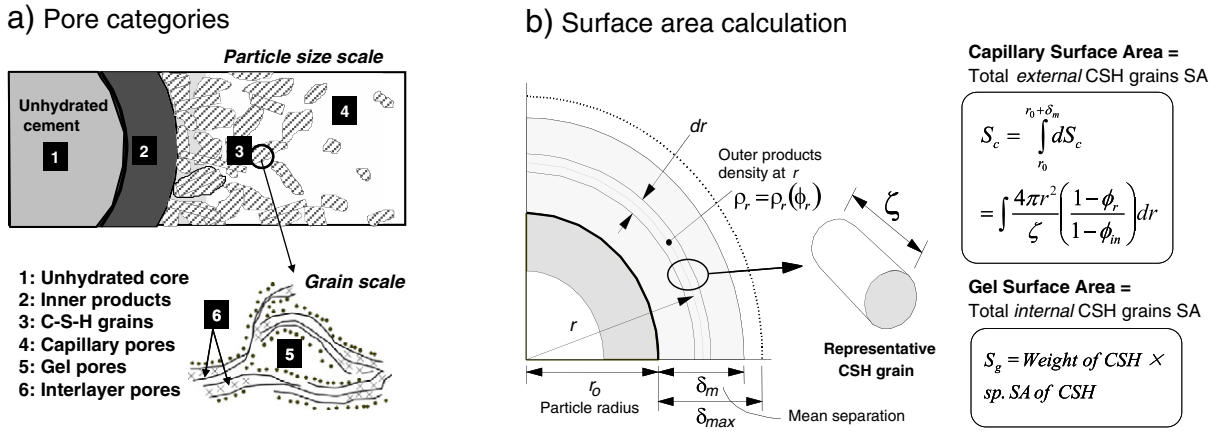

Fig. 1. Microstructure model [21].

interlayer pores is used as assessment of pore size distribution, according to the following equation.

$$\phi(r) = \phi_{lr} + \phi_{gl}\cdot\left(1-\exp\left(-B_{gl}r\right)\right) + \phi_{cp}\cdot\left(1-\exp\left(-B_{cp}r\right)\right) \quad (5)$$

Hence, based on the above equations, both the porosity of categorized pores and their size distribution are computed, and they are utilized to describe the microstructure of the matrix. Furthermore, this information provides the basis for models of other properties, such as strength, moisture loss, shrinkage and creep. In this paper, the strength model is also modified to accommodate BFS, so it is briefly introduced in Section 2.2.

2.2. Strength model based on capillary porosity

In DuCOM, a strength model that was proposed by Otabe et al. [21,23] is utilized. This model follows the concept proposed by Schiller [24], in which both the present and initial capillary porosity are taken into account based on their ratio. The model has been verified for Portland cement concrete. In general, it is assumed that the strength of concrete or mortar is principally related to capillary porosity development, because capillary pores are much larger than gel and interlayer pores and influence strength more significantly. The strength (f_c) of concrete or mortar follows the following equation:

$$f_c = f_\infty\left[1-exp\left\{-\alpha\left(k\cdot\frac{D_{hyd.out}}{\theta}\right)^{\beta}\right\}\right] \quad (6)$$

where f_∞ is the ultimate strength when capillary pores are completely filled in. k is the coefficient considering the effect of temperature to microstructure change of hydrates. α and β are material constants. $D_{hyd.out}$ is the ratio of filled capillary porosity to initial capillary porosity. θ is the coefficient considering the contribution of the water-to-powder ratio to strength at the same capillary porosity ratio $D_{hyd.out}$.

For Portland cement, f_∞ is not constant but related to chemical fractions of clinkers, i.e. C_3S and C_2S. This is because the micro-strength of gel grains may also influence the macro-strength of concrete through variations in chemical composition or internal pore structure. For example, cement containing more C_2S has higher strength at a later age, which may be attributed to a lower Ca/Si ratio of C–S–H grains and higher micro-strength. Therefore f_∞ is given by

$$f_\infty = A\frac{p_{C_3S}}{p_{C_3S}+p_{C_2S}} + B\frac{p_{C_2S}}{p_{C_3S}+p_{C_2S}} \quad (7)$$

$D_{hyd.out}$ is computed by the following equation:

$$D_{hyd.out} = \frac{\phi_{cp.ini}-\phi_{cp}}{\phi_{cp.ini}} \quad (8)$$

where p_{C3S} and p_{C2S} are fractions of C_3S and C_2S respectively, and A and B are the ultimate strength of C_3S and C_2S, which are assumed to be 215 MPa are 250 MPa. $\phi_{cp.ini}$ is the initial capillary porosity just before setting, and ϕ_{cp} is the current capillary porosity, and therefore $\phi_{cp.ini}-\phi_{cp}$ are the voids filled by hydrate.

Hence, capillary porosity dominates strength development according to Eq. (8). This strength model provides a common evaluation for cementitious materials, i.e. as long as capillary porosity is well simulated, strength can be predicted and compared for PC and BFS. However, as introduced in Section 1, the pore structure in DuCOM has not been investigated for BFS, so whether the strength model can be applied to BFS is still unknown. On the other hand, the strength model is related to only capillary porosity but is independent of the pore size distribution. Therefore, if we start the research from the relationship between strength and porosity, the influence of pore size distribution can be avoided, simplifying the verification process. As the starting point, the authors designed some experiments related to the porosity and strength of BFS. Corresponding analysis is carried out in the following section.

3. Study on porosity

3.1. Test program

In DuCOM, as shown in Eq. (1), capillary porosity is principally dominated by three micro–hygro–physical properties, including the hydration degree of cementitious powder, the volume of chemically combined water, and the pore volume inside gel grains, i.e. α, β and ϕ_{ch}. Therefore, when we study the capillary porosity by experiment, it is helpful to check these properties. Measurement of the hydration degree and chemically combined water is not difficult to conduct. As to the pore volume, as equivalent, the authors decided to measure the water content under saturated condition.

Two groups of specimens were prepared, consisting of both PC and BFS. In the PC group, pure cement pastes made of ordinary Portland cement (N), medium heat cement (M) and low heat cement (L) with w/c ratio of 0.5 were cast respectively. Meanwhile, the cement pastes adopted above were replaced by 45% blast furnace slag for the BFS group, with the resulting pastes named NB, MB, and LB. The chemical and physical properties of the cement and BFS are detailed in Table 1. The size of these specimens were $4\times4\times16$ cm and they were sealed for 1 day after casting. Then the specimens were cut into pieces 3 mm deep and cured in water under normal temperature (20 °C) until the test ages. After that, the degree of hydration, chemically combined water, and physical water were tested, respectively.

The degree of hydration was measured by the XRD method. Physical water was categorized into capillary water and water inside gel grains, i.e. gel and interlayer water. In experiments, it is impossible to divide capillary, gel and interlayer water precisely. Hence the authors define the capillary, gel and interlayer water in the test as shown in Fig. 2: first, specimens with saturated condition were dried at 40 °C and the weight loss was considered as the total capillary water. The remaining physical water was regarded as the sum of the gel and interlayer water. Then the specimens were exposed at 105 °C to remove all the gel and interlayer water. The weight loss from 40 °C to 105 °C was measured as gel and interlayer water. Finally, the

Table 1
Mineral composition and properties of materials.

	Density (g/cm^3)	Blaine (cm^2/g)	Mineral composition determined by Rietveld method (%)						
			C_3S	C_2S	C_3A	C_4AF	Gypsum	Hemihydrate	Anhydrite
N	3.16	3180	61.2	16.7	3.9	13.6	0.3	3.2	
M	3.23	3100	47.2	28.9	1.5	16.9	2.1	2.0	
L	3.26	3390	34.0	46.0	2.0	13.0			4.0
	Density (g/cm^3)	Blaine (cm^2/g)	Chemical composition (%)						
			SiO_2	Al_2O_3	Fe_2O_3	CaO	MgO	TiO_2	SO_3
BFS	2.91	4370	33.0	14.44	0.79	42.03	6.06	0.41	1.81

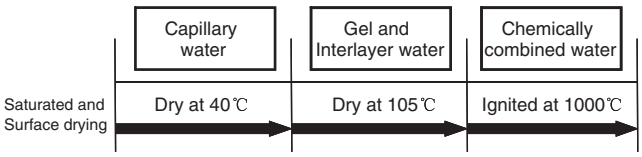

Fig. 2. Definition of physical and chemically combined water in test.

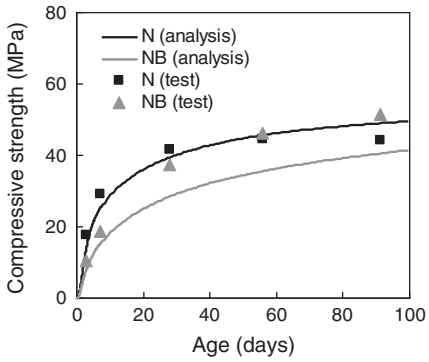

Fig. 3. Comparison of strength development.

specimens were heated up to 1000 °C to remove chemically combined water. The weight percentage is defined as the lost water to remaining paste weight after heating at 1000 °C.

The definition of the gel and interlayer water needs to be clarified. As the definition in the test, the specimens were dried at 40 °C to remove capillary pore water and then exposed at 105 °C to measure the gel and interlayer water loss. Actually, after drying at 40 °C, a little water still remained in capillary pores while some of the gel water evaporated. Therefore, strictly speaking, the gel and interlayer water measured do not coincide completely with the analysis in Section 3.2. However, since only a small part of the gel water was lost during drying at 40 °C, it can be reasonably assumed that the test result is approximately comparable with the computed value.

Besides, mortar specimens of size $\phi 5 \times 10$ cm were cast for the compressive strength test according to JIS A1108. The surface dry density of fine aggregate was 2.67 g/cm^3 and the volume ratio in the paste was around 50%.

3.2. Test results and analysis based on current model

Analysis based on the current model was also conducted for PC and BFS. In DuCOM, the inputs included the initial mix proportions, material properties, casting temperature, specimen geometry and the boundary conditions to which the specimens were exposed. The analysis involved a dynamic coupling of cement hydration, microstructure formation and moisture transport into finite element computation. Relative information such as the degree of hydration, porosity and pore size distribution, and internal moisture were output. For strength development, calculation followed the model in Section 2.2. From the multi-component hydration model, chemically combined water from total powder and that from slag could be computed respectively.

The ratio (f_{wgel}) of gel and interlayer water is calculated by the following equation:

$$f_{wgel} = \left(\phi_{gl} + \phi_{lr}\right) \cdot S_{iner} \cdot \rho_w / W_p \tag{9}$$

The gel and interlayer water ratios from slag hydration (f_{wgel_sg}) are obtained with the following equations:

$$f_{wgel\_pc} = \frac{\alpha_{pc} W_{p\_pc}}{1-\phi_{ch}} \cdot \phi_{ch} \cdot S_{iner} \cdot \rho_w / W_p \tag{10}$$

$$f_{wgel\_sg} = f_{wgel} - f_{wgel\_pc} \tag{11}$$

where f_{wgel}, f_{wgel_pc} and f_{wgel_sg} are the gel and interlayer water ratios from total powder, Portland cement and slag, respectively. α_{pc} is the degree of hydration of Portland cement and W_{p_pc} is the weight of Portland cement per unit paste volume. ϕ_{ch} is the intrinsic porosity of gel grains, which is the constant 0.33. S_{iner} is the average saturation of gel and interlayer pores, and ρ_w is the density of pore water, which is considered to be 1.00 g/cm^3.

The test results and analysis are shown in Figs. 3–6. As shown in Fig. 3, the strength of N is predicted accurately, while NB is underestimated at a later age. In the test, NB had lower strength at an early age, but reached higher strength at 91 d as hydration went on. However, in the analysis, NB is always lower than N. Therefore, the current model cannot proper evaluate strength development of BFS at a later age. The authors assume that this may be due to overestimation of capillary porosity at a later age. In order to gain higher strength, more capillary pores should be filled by hydrates.

For the degree of hydration, Fig. 4 shows good agreement with the test results for both N and NB. The hydration degree of BFS is always lower than that of PC, which is consistent with past research. As to chemically combined water, as Fig. 5 shows, although analysis gives slightly higher results for both cases, the trend during the whole hydration process can be traced accurately. Hence it can be seen that the current model provides good prediction for both the hydration degree and chemically combined water and neither is the cause of the discrepancy in strength.

Fig. 6 shows a comparison of the gel and interlayer water ratio versus the chemically combined water ratio. The chemically combined water ratio reflects the hydration process. For N, good

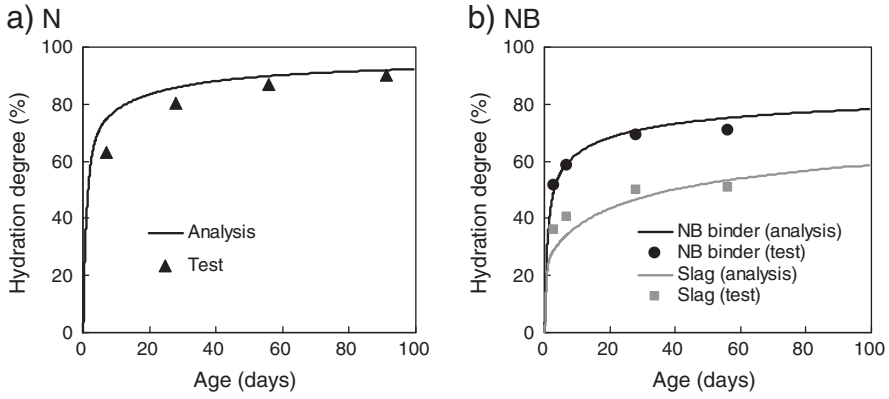

Fig. 4. Comparison of hydration degree.

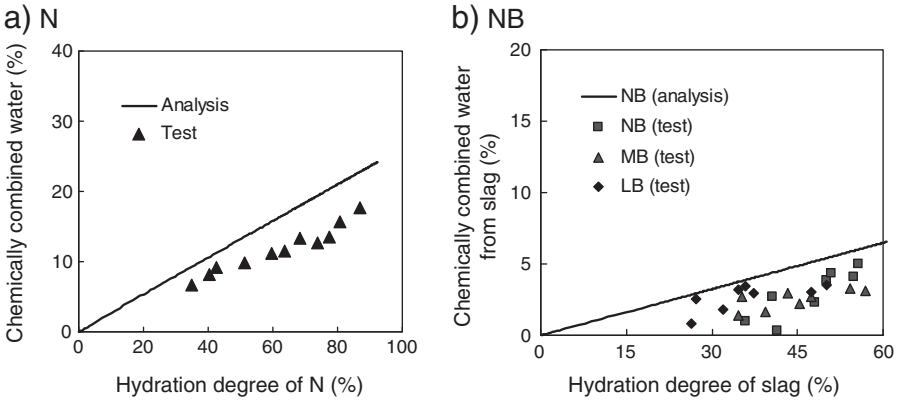

Fig. 5. Comparison of chemically combined water.

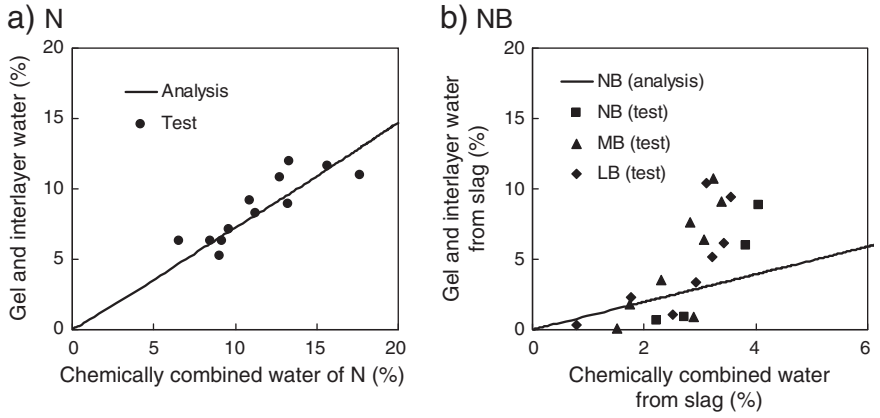

Fig. 6. Comparison of gel and interlayer water.

agreement is obtained, but for NB, the analysis apparently underestimates gel and interlayer water development at a later age. Unlike the linear increase in N, all the BFS test data show a tendency toward nonlinear increase, with higher gel and interlayer water content gain at a later age. However, the analysis gives a linear increase for NB. Therefore it is rational to deduce that the current model is only applicable to PC rather than BFS due to inconsistent gel and interlayer pore water assessment. This inconsistency leads to underestimation of gel and interlayer porosity, and therefore overestimation of capillary porosity for BFS, which is also the cause of discrepancy of strength in Fig. 3.

3.3. Enhanced model on porosity

The test data in Fig. 6 indicates that BFS paste tends to contain more gel and interlayer water at a higher degree of hydration, which implies larger porosity inside gel grains at a later age. Hence, the value of ϕ_{ch}, which represents the intrinsic porosity of gel grains, needs to be reevaluated. It may not be a constant but a variable that is related to slag replacement and the degree of hydration. Here, in order to describe the role of slag on the intrinsic porosity, an index is proposed as follows:

$$\tau = \frac{f_{sg}\alpha_{sg}}{f_{pc}\alpha_{pc}} \tag{12}$$

where f_{pc} and f_{sg} are weight fractions of Portland cement and BFS, α_{pc} and α_{sg} are their degrees of hydration. Therefore, $f_{pc}\alpha_{pc}$ and $f_{sg}\alpha_{sg}$ represent the amount of hydrates produced by Portland cement and BFS, respectively. Index τ is the ratio of hydrates from BFS to those from Portland cement.

Based on the above, a new development of intrinsic porosity ϕ_{ch} is proposed as the following equation:

$$\phi_{ch} = 0.45 - 0.12 \cdot \exp\left(-0.38 \cdot (\tau)^{3.0}\right) \tag{13}$$

The function ϕ_{ch} versus τ is illustrated in Fig. 7. When τ increases, which means the proportion of BFS hydrates becomes larger, ϕ_{ch} increases, thus more gel and interlayer pores are gained. τ is related to the slag ratio and hydration degree of slag. When the slag ratio or degree of hydration increases, based on Eq. (12), the value of τ increases and therefore higher ϕ_{ch} is obtained.

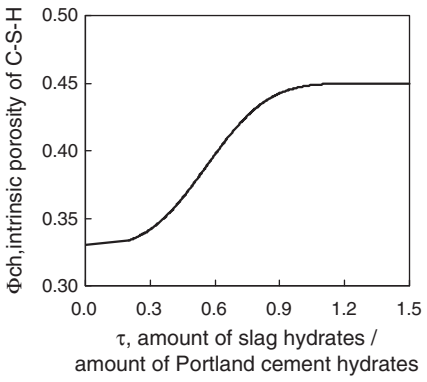

Fig. 7. Relationship between τ and ϕ_{ch}.

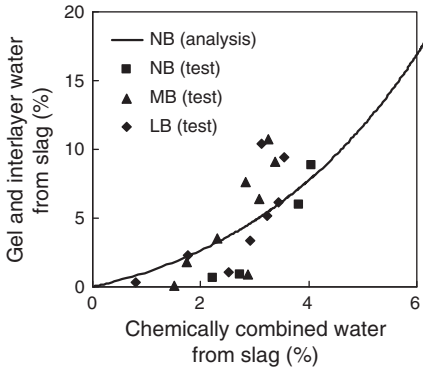

Fig. 8. Gel and interlayer water of NB based on enhanced model.

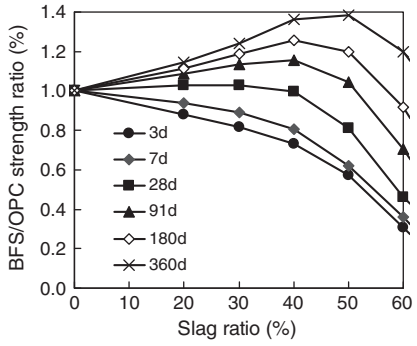

Fig. 10. BFS/OPC strength ratio based on enhanced model (w/p = 0.5).

With the enhanced model, the gel and interlayer water content ratio is calculated again and shown in Fig. 8. It is obvious that the enhanced model shows nonlinear increase and higher gel and interlayer water at a later age, which is consistent with the test results. Therefore, from the viewpoint of micro-physical properties of the matrix, the enhancement on the intrinsic porosity provides better simulation for BFS.

3.4. Verification

Before verification by strength test, another modification needs to be mentioned for the ultimate strength in Eq. (7), in order to consider the contribution of the micro-strength of C–S–H gel grains. It is reported that C–S–H of BFS has a lower Ca/Si ratio [25–28], which may contribute to gel grains and induce higher grain strength. Therefore, Eq. (7) is revised as follows:

$$f_\infty = \left(A\frac{p_{C_3S}}{p_{C_3S}+p_{C_2S}} + B\frac{p_{C_2S}}{p_{C_3S}+p_{C_2S}} \right)\cdot p_{pc} + C\cdot p_{sg} \tag{14}$$

where C is the ultimate strength factor of slag, assumed as 260 MPa. Finally, the verifications by strength test are shown in Fig. 9. In the analysis at the early age, the strength of BFS was less than PC, BFS tended to gain higher strength at later age as hydration progressed, which agrees with the test well. The strengths of BFS with various slag ratios at different ages are compared in Fig. 10. The vertical axis represents the strength ratio of BFS to OPC at the same age. At an early age such as 3 d or 7 d, strength decreases as the slag ratio increases. This may be attributed to the lower degree of hydration. As the age increases, obviously the strength of BFS with higher slag ratios increases faster, and at a late age such as 360 d, the maximum value of strength lies in the range of 40% to 50% slag ratios. During this stage, the increase in gel and interlayer porosity and decrease in capillary porosity plays more important role in strength development. The higher the slag ratio, the faster intrinsic porosity increases. However, with regards to a slag ratio higher than 50%, although intrinsic porosity increases fastest, due to the lower degree of hydration, the ultimate strength ratio is less. Therefore, it can be concluded that strength is influenced by both the degree of hydration and the pore structures. For higher slag ratios, the degree of hydration becomes smaller while the pore structure tends to be denser (contains more gel and interlayer pores), implying both negative and positive effects. Therefore, the ultimate strength in the mid range of replacement is the highest. The experiment result [29] shown in Fig. 11 indicates the validity of the enhanced model.

4. Study of pore size distribution

4.1. Moisture loss test under different curing time

In Section 3, the microstructure model has been modified in terms of porosity. However, some properties such as moisture loss depend on not only porosity but also pore fineness, i.e. pore size distribution. A cement matrix with the same porosity but finer pores is more capable of retaining water under drying condition. Hence, when we deal with the macrostructure of BFS, it is also necessary to investigate the modeling of pore size distribution and its relationship with moisture loss.

First the authors conducted the moisture loss test. Materials similar to those used for the porosity investigation were adopted. OPC and BFS mortar prism specimens measuring 4×4×16 cm were prepared. The slag ratios were 20% and 40%, respectively, and the water-to-powder ratio was 0.50. The sand volume ratio was 40%. The mix proportions are shown in Table 2. For each mix proportion, three identical specimens were cast for the test. The mixing procedure was carried out following the JSCE standard. After demolding, the specimens were sealed and stored under the constant temperature of 20 °C until the ages of 1 d, 3 d, 7 d and 28 d, respectively. Then the

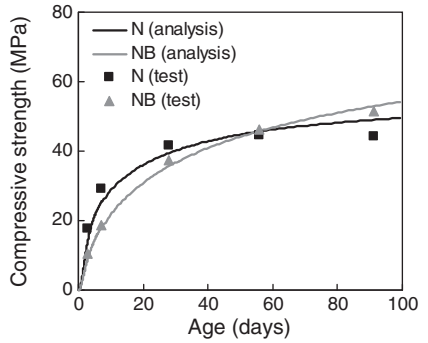

Fig. 9. Comparison of strength development based on enhanced model.

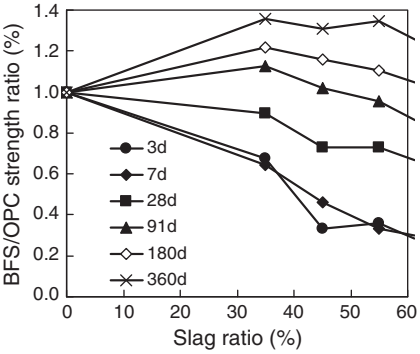

Fig. 11. BFS/OPC strength ratio with slag ratio from experiment [29].

Table 2
Mix proportion.

Group Name	Water (kg/m^3)	Cement (kg/m^3)	BFS (kg/m^3)	Sand (kg/m^3)	Water/Powder	BFS/Powder
N	367	735	0	1040	0.5	0
BB20	365	584	146	1040	0.5	20%
BB40	362	435	290	1040	0.5	40%

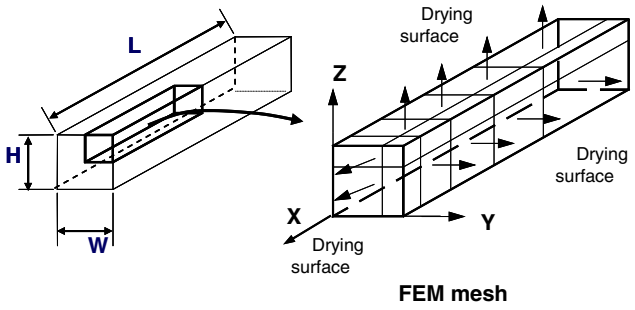

Fig. 12. FEM mesh for analysis.

specimens were exposed at RH 60% and the ambient temperature was kept constant. The weight of water loss during drying was measured.

Meanwhile, analysis of moisture loss was conducted with the enhanced model of porosity and original treatment of pore size distribution. The same conditions for the specimens and test environment were applied. The meshing in the analysis is illustrated in Fig. 12. Since moisture loss behavior is closely related to water movement and equilibrium in pore structures, which is simulated by the moisture transport and equilibrium model in DuCOM, this model is also utilized in the analysis. The authors assume that the water movement and equilibrium in micro-pores obey the same principle for PC and BFS, so the moisture transport and equilibrium model is not modified in this research. Therefore, the introduction of this model is omitted.

4.2. Test results and analysis based on current model

Fig. 13 shows the results of test and analysis. For short time curing such as 1 d, 3 d and 7 d, analysis provides good agreement with test results, i.e. BFS loses more water than OPC. On the other hand, for longer curing times up to 28 d, the opposite tendency is observed between analysis and test. Analysis still shows higher moisture loss for BFS, while the test results reveal that BFS tends to lose less water. The authors suppose that this discrepancy may derive from the model of pore fineness, so it is necessary to examine the pore size distribution evolution.

As discussed in Section 1, it has been widely reported that the pore size distribution of the BFS matrix is quite different from that of PC. Generally speaking, at a very early age, the BFS matrix has a coarse pore structure, while as hydration goes on, it tends to be finer than OPC at a later age. Fig. 14 presents an example of the pore size distribution curve for BFS and OPC paste measured by the MIP method [15]. At an early age such as 3 d, most of the pores in the BFS matrix lie in the range of 80 nm to 800 nm, which is much coarser than OPC. At 28 d, the volume of pores with a radius larger than 50 nm is similar to that of OPC, but a large volume of pores with a radius smaller than 25 nm exist. At 24 weeks, most of the pores have a radius smaller than 10 nm, which is denser than OPC. Fig. 15 presents the analysis by the current microstructure model. At an early age such as 1 d, the BFS matrix has a coarser pore

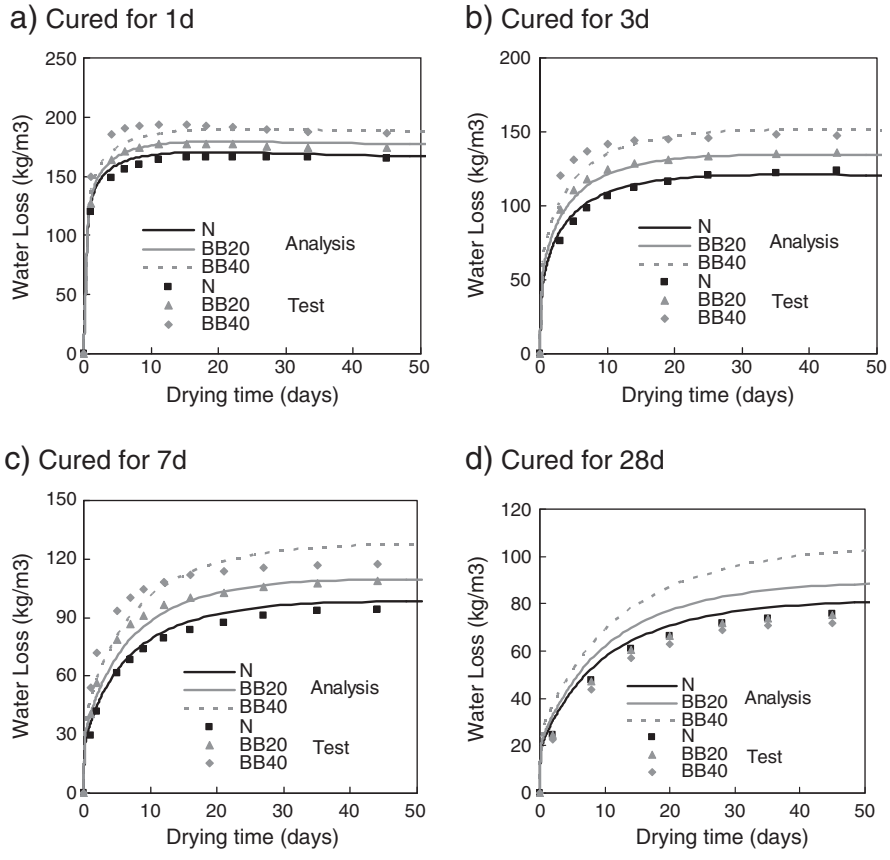

Fig. 13. Water loss analysis based on original pore size distribution.

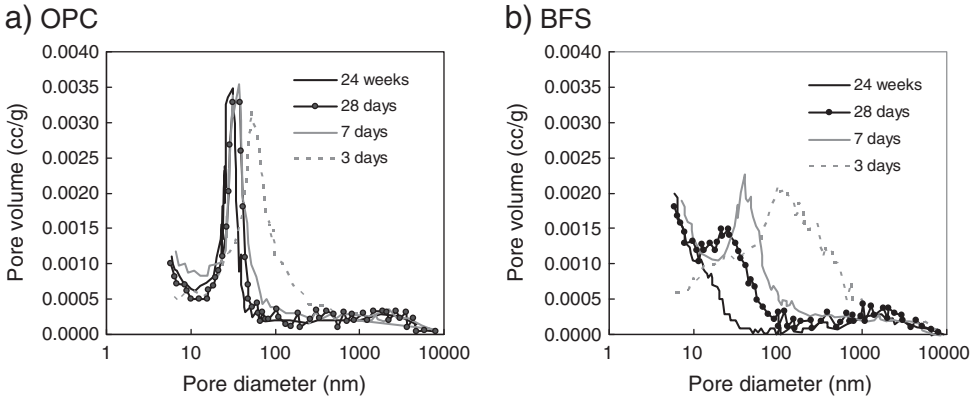

Fig. 14. Pore size distribution of BFS and OPC measured by MIP [15].

distribution, but at 24 weeks, the peak of the curve is in a similar position, which means that the pore size estimates are similar. Here it has to be mentioned that the microstructure model in DuCOM is a more ideal treatment than the true matrix, so quantitatively the pore size distribution curve by analysis cannot be compared with the test by the MIP method. However, qualitative comparison between Figs. 14 and 15 indicates that the current model does not reflect the principle distinction between BFS and OPC. This may be the reason for the discrepancy in moisture loss at 28 d. Therefore, the current pore size distribution model needs to be modified.

4.3. Enhancement on pore size distribution

According to the microstructure model in Section 2.1, it is known that the pore size distribution depends on both porosity and surface area. In Section 3, the enhanced porosity model has been modified to provide reasonable information on porosity. Therefore the discussion turns to the surface area of capillary and gel pores, which is calculated in Eq. (2). It is possible that the surface areas are underestimated.

Here, two intrinsic parameters need to be paid attention, i.e. ζ and s_g. It seems that ζ and s_g are keys for modifying pore size distribution. ζ represents the dimension of individual gel grains. When its value decreases, according to Eq. (2), the surface area of capillary pores increases. This is not difficult to understand, because if capillary pores are filled in by smaller gel grains, their surface area becomes larger and thus finer distribution is expected. Similarly, a larger surface area and finer distribution of gel pores are available with higher values of s_g.

Therefore, denser pore size for BFS at a later age can be achieved by decreasing the value of ζ and increasing s_g in the model at a higher degree of hydration. Actually, this treatment has clear physical meaning. In the Portland cement matrix, CH crystals with larger size than C–S–H gels exist. In the case of BFS, due to hydration of slag, some CH was consumed and more C–S–H gels filled in capillary pores.

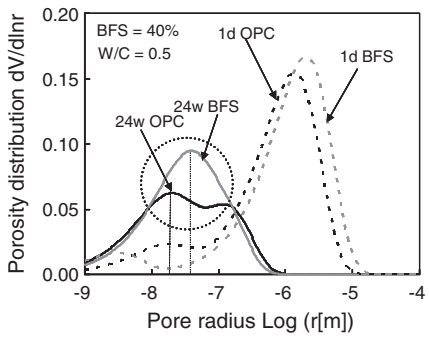

Fig. 15. Pore size distribution based on current model.

Hence, the average particle size in the paste decreased and surface area of capillary pores increased. As to gel pores, Richardson et al. [30] reported that for OPC or a low slag ratio, C–S–H has a fibrillar-like morphology, while the morphology of high slag ratio tends to be of the crumpled-foil type. This implies a transition of hydrates from essentially one-dimensional growth to two-dimensional, resulting in higher tortuosity and specific surface area in gel pores. Therefore, increasing s_g is consistent with the past research.

Therefore, the enhanced pore distribution model is proposed. For C–S–H formed from slag hydration, its grain size (ζ^{sg}) and specific surface area (s_g^{sg}) are given by the following equations

$$\zeta^{sg} = -0.9\cdot\alpha_{sg} + 1.0 \tag{15}$$

$$s_g^{sg} = 1500\cdot\alpha_{sg}^2 \tag{16}$$

where the unit of ζ^{sg} and s_g^{sg} are 10^{-8} m and 10^3 m^2/kg, respectively. ζ^{sg} and s_g^{sg} are functions of the slag hydration degree.

Considering the weight fractions of Portland cement and slag, the average grain size and specific surface area of gel pores are calculated by the following equations:

$$\zeta = 1 \Big/ \left(\frac{f_{pc}}{\zeta^{pc}} + \frac{f_{sg}}{\zeta^{sg}}\right) \tag{17}$$

$$s_g = s_g^{pc} f_{pc} + s_g^{sg} f_{sg} \tag{18}$$

In Eqs. (15) and (16), for gels generated from slag hydration, ζ^{sg} and s_g^{sg} are dependent variables versus the hydration degree of slag. On the other hand, for gels generated from Portland cement, ζ^{pc} and s_g^{pc} are assumed to be the same values as those of the original model, and thus to be constant. The average values of ζ and s_g for the total powder are obtained by the weight fractions of Portland cement and slag. Hence, ζ and s_g are also dependent variables versus hydration degree.

In the enhanced model, Eq. (2), which describes the calculation of capillary and gel surface areas, is changed by the discretization method in time domain as follows:

$$\begin{aligned} S_c^n &= S_c^{n-1} + \Delta S_c = S_c^{n-1} + \frac{4\pi r^2}{\zeta}\left(\frac{1-\varphi_r}{1-\varphi_{in}}\right) \\ S_g^n &= S_g^{n-1} + \Delta S_g = S_g^{n-1} + \left(W_g^n - W_g^{n-1}\right)\cdot s_g \end{aligned} \tag{19}$$

where S_c^n and S_g^n are the capillary and gel surface areas at time step n, and S_c^{n-1} and S_g^{n-1} are the capillary and gel surface areas at time step $n-1$. W_g^n and W_g^{n-1} are the gel weight at time steps n and $n-1$, respectively. r^n and r^{n-1} are the outer product radius at time steps n and $n-1$.

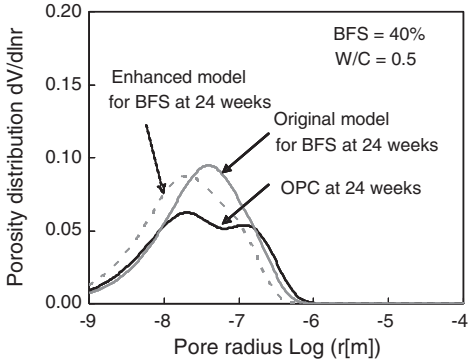

Fig. 16. Pore size distribution based on enhanced model.

Based on Eq. (19), at time step *n*, the capillary and gel surface area increases, ΔS_c and ΔS_g, produced during the time interval, are computed separately. Then the total surface areas are integrated in the whole time domain. Therefore, the new gel grain size and specific gel surface area in Eqs. (17) and (18) correspond to the gel produced in time step *n*.

In the enhanced model, individual gel grains at a higher degree of hydration become smaller, leading to denser capillary pore distribution at a later age. In the case of gel pores, since the surface area increases by s_g, the pore structure also becomes finer. Therefore, a finer microstructure can be achieved for the BFS matrix, which qualitatively agrees with the test by the MIP method. The size distribution in Fig. 15 for the 24 weeks case is calculated again and showed in Fig. 16. For matured paste, the peak of the BFS size distribution curve obviously moves toward a finer direction.

4.4. Verification

It would be persuasive if the enhanced model could be verified by the pore structure test quantitatively. The morphology image by electron microscope supports the enhanced model but cannot provide quantitative verification. Although the MIP method provides proof of a denser pore structure, it is not believed to provide "true" porosity because the pore structure may be altered during mercury intrusion. On the other hand, since the water content inside the pore structure is strongly influenced by its fineness or surface area, the water isotherm test is applicable for verification. In past research, the water isotherm of the PC matrix has been simulated by DuCOM and good agreement with the test was obtained. When BFS is investigated, the water isotherm test can also be used as verification. In this section, modeling of pore size distribution is verified by the water sorption isotherm obtained by Maruyama et al. [31].

In the test, the OPC and BFS matrices with w/p ratio of 0.55 were cured for 150 d and then a water desorption test was carried out until RH lower than 0.4, at which time most of the gel and capillary water was considered to have evaporated. The same environment condition was applied in the analysis. The pore size models before and after enhancement were utilized, and they were compared with the test results in Fig. 17. Obviously, the analysis based on the enhanced model is in better agreement with the test data. The BFS matrix keeps more water than OPC at the same RH, which implies a higher surface area and finer pore structure.

Analysis of moisture loss was carried out again, and the results are shown in Fig. 18. With the enhanced model, the different trends from OPC can be traced. If exposed under drying condition after short term curing, the BFS matrix loses more water. With a longer curing time such as 28 d, BFS mortar tends to retain more water.

With enhancement of the porosity and pore size distribution, it is considered that now the microstructure of the BFS matrix can be properly simulated in DuCOM. Therefore, except for moisture loss, drying shrinkage of BFS concrete is simulated. This simulation is carried out through combination with a multi-scale constitutive model of solidifying cementitious composites, which deals with shrinkage and creep simulation in DuCOM [21]. The analyses of drying shrinkage based on the original and enhanced models are shown in Figs. 19 and 20. The analysis using the enhanced model agrees better with the test data [32,33] , and BFS is found to have larger shrinkage than OPC due to finer pore distribution and larger capillary tension force.

5. Summary and conclusions

This study investigated the microstructure model of the BFS matrix. First, experiments on the strength and selected micro–hygro–physical properties were conducted. Combined with the strength test, it was found that the strength development of BFS concrete is underestimated at a later age. Therefore, the degree of hydration, chemically combined water, and gel and interlayer water were compared with the test results. The authors found that the gel and interlayer water content is underestimated in the model, which causes overestimation of capillary porosity and strength discrepancy. Hence, an enhanced intrinsic porosity model was proposed for the BFS matrix. As the degree of hydration increases, more gel and interlayer pores are gained and hydration product fills in the capillary pores more efficiently, resulting in higher strength in a later age. Verification

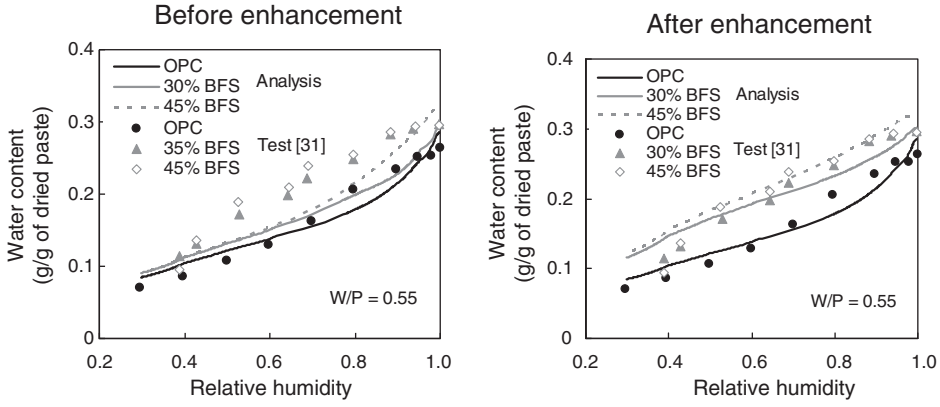

Fig. 17. Comparison of water desorption.

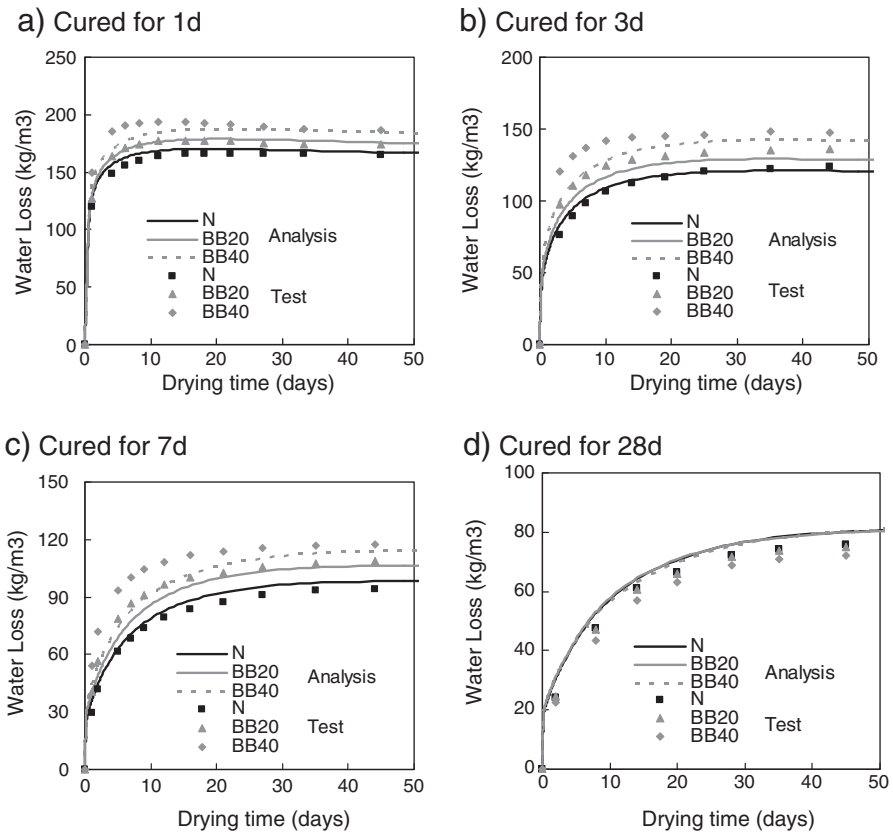

Fig. 18. Water loss analysis based on enhanced model.

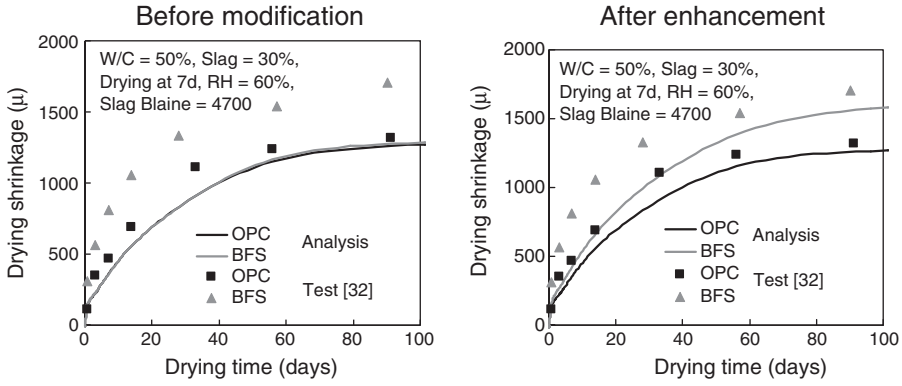

Fig. 19. Comparison of short-time drying shrinkage.

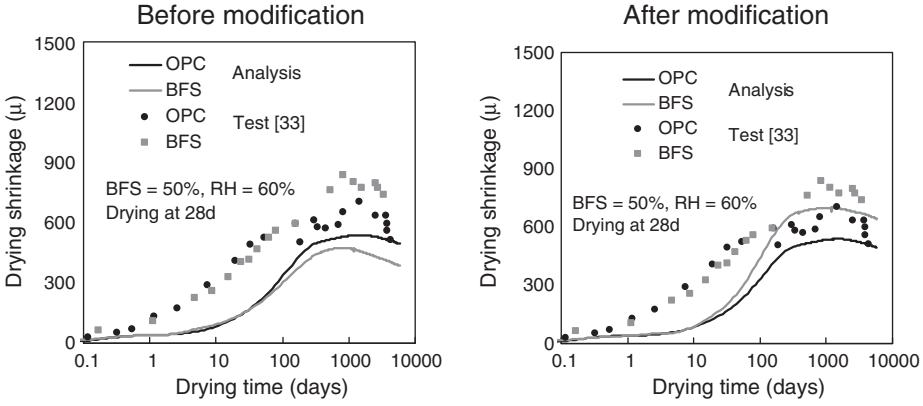

Fig. 20. Comparison of long-time drying shrinkage.

by strength experiment showed good agreement. Furthermore, the pore size distribution model was studied and moisture loss tests were conducted. It was found that the moisture loss of BFS at a later age is overestimated, and thus the pore size distribution model was investigated. The authors found that based on the surface area computed by the current model, the pore structure of the BFS matrix at a later age becomes too coarse. Two key parameters representing the equivalent gel size and specific surface area of gel pores were studied in detail, and it was found that they are closely related to pore fineness. Hence, an enhanced pore distribution model capable of accurate simulation of the finer pore structure of the BFS matrix at a later age was proposed. Verification was conducted by water desorption curve and moisture test and the results showed good improvements.

References

[1] J.J. Brooks, Elasticity, creep, and shrinkage of concretes containing admixtures, ACI Special Publication 194 (2000) 283–360.
[2] E. Tazawa, S. Miyazawa, Influence of cement and admixture on autogenous shrinkage of cement paste, Cement and Concrete Research 25 (2) (1995) 281–287.
[3] K.M. Lee, H.K. Lee, S.H. Lee, G.Y. Kim, Autogenous shrinkage of concrete containing granulated blast-furnace slag, Cement and Concrete Research 36 (7) (2006) 1279–1285.
[4] K. Luke, F.P. Glasser, Selective dissolution of hydrated blast furnace slag cements, Cement and Concrete Research 17 (2) (1987) 273–282.
[5] J.S. Lumley, R.S. Gollop, G.K. Moir, H.F.W. Taylor, Degrees of reaction of the slag in some blends with Portland cements, Cement and Concrete Research 26 (1) (1996) 139–151.
[6] E. Demoulian, P. Gourdin, F. Hawthorn, C. Vernet, Influence of slags chemical composition and texture on their hydraulicity, Proceedings of 7th International Congress on the Chemistry of Cement, vol. 2, 1980, pp. 89–104.
[7] A.F. Battagin, Influence of degree of hydration of slag on slag cement, Proceedings of the 9th International Congress on the Chemistry of Cement, 3, 1992, pp. 166–172.
[8] E. Sakai, H. Imoto, M. Daimon, Hydration and strength development of blast furnace slag cement, Proceedings of JCI 26 (1) (2004) 135–140 (In Japanese).
[9] M. Regourd, Microstructure of cement blends containing fly ash, silica fume, slag and fillers, Materials Research Society Symposium Proceedings 85 (1987) 187–200.
[10] J.I. Escalante-Garcia, J.H. Sharp, The microstructure and mechanical properties of blended cements hydrated at various temperatures, Cement and Concrete Research 31 (5) (2001) 695–702.
[11] K. Tan, X. Pu, Strengthening effects of finely ground fly ash, granulated blast furnace slag, and their combination, Cement and Concrete Research 28 (12) (1998) 1819–1825.
[12] R.F. Feldman, Pore structure formation during hydration of fly ash and slag cement blends, effects of fly ash incorporation in cement and concrete, Proceedings of Materials Research Society (1981) 124–133.
[13] Q.L. Feng, E.E. Lachowski, F.P. Glasser, Densification and migration of ions in blast furnace slag-portland cement pastes, Materials Research Society Symposium Proceedings 136 (1989) 263–272.
[14] C.M. Aldea, F. Young, K. Wang, Effects of curing conditions on properties of concrete using slag replacement, Cement and Concrete Research 30 (3) (2000) 465–472.
[15] D. Kwak, A fundamental study on pore structure affecting carbonation of concrete, Ph.D. thesis, Tokyo Metropolitan University, 2004. (In Japanese).
[16] Y. Dan, T. Iyoda, Y. Ohtsuka, Y. Sagawa, The relationship between curing condition and durability on concrete using blast-furnace slag cement, Division E, Journals of JSCE 65 (4) (2009) 431–441 (In Japanese).
[17] F.J. Hogan, J.W. Meusel, Evaluation for durability and strength development of a ground granulated blast furnace slag, Cement, Concrete and Aggregates 3 (1) (1981) 40–52.
[18] J.J. Brooks, P.J. Wainwright, M. Boukendakji, Influence of slag type and replacement level on strength, elasticity, shrinkage and creep of concrete, ACI Special Publication 132 (1992) 1325–1341.
[19] J. Li, Y. Yao, A study on creep and drying shrinkage of high performance concrete, Cement and Concrete Research 31 (8) (2001) 1203–1206.
[20] J.C. Chern, Y.W. Chan, Deformations of concretes made with blast-furnace slag cement and ordinary portland cement, ACI Materials Journal 86 (4) (1989) 372–382.
[21] K. Maekawa, T. Ishida, T. Kishi, Multi-scale modeling of structural concrete, Taylor & Francis, 2008.
[22] Y. Luan, T. Ishida, T. Nawa, T. Sagawa, Enhanced hydration model and simulation of hydration process of blast furnace slag in blended cement, Proceedings of JCI 33 (1) (2011) 71–76 (In Japanese).
[23] Y. Otabe, T. Kishi, Hydration and strength development model for quality prediction and support on construction management, Seisankenkyu 57 (2) (2005) 37–44 (In Japanese).
[24] K.K. Schiller, Mechanical properties of non-metallic materials, Butterworths, London, 1958, pp. 35–50.
[25] B. Talling, J. Brandstetr, Present state and future of alkali-activated slag concretes, Fly Ash, Silica Fume, Slag and Natural Pozzolans in Concrete, 1989, pp. 1519–1545.
[26] I.G. Richardson, G.W. Groves, Microstructure and microanalysis of hardened cement pastes involving ground granulated blast-furnace slag, Journal of Materials Science 27 (1992) 6204–6212.
[27] M. Regourd, B. Mortureux, H. Hornain, Use of condensed silica fume as filler in blended cements, ACI Special Publication 79 (1983) 847–866.
[28] A.M. Harrisson, N.B. Winter, H.F.W. Taylor, Microstructure and microchemistry of slag cement pastes, Materials Research Society Symposium Proceedings 85 (1986) 213–222.
[29] Y. Endo, Influence of slag on mix proportion and strength development of concrete, Proceedings of Application of Slag in Concrete Symposium, JSCE (1987) 29–36 (In Japanese).
[30] I.G. Richardson, Tobermorite/jennite and tobermorite/calcium hydroxide-based models for the structure of C–S–H: applicability of hardened pastes of tricalcium Silicate, β-dicalcium silicate, portland cement, and blends of portland cement with blast-furnace slag, metakaolin, or silica fume, Cement and Concrete Research 34 (9) (2004) 1733–1777.
[31] I. Maruyama, N. Kishi, Disjoining pressure of hardened cement paste using blast-furnace slag, Proceedings of AIJ Tokai Chapter Architectural Research Meeting 48 (2010) 41–44 (In Japanese).
[32] S. Asamoto, M. Kato, Investigation into shrinkage behaviors of mortar with blast-furnace slag based on microstructures, Sustainable infrastructure development in Asia, International Exchange Symposium, Sri Lanka, 2009.
[33] J. Ozaki, K. Sugada, Long time creep and shrinkage experiment of concrete, Proceedings of JCI 20 (2) (1998) 685–690 (In Japanese).